Journal of Engineering Science and Technology
24th EURECA 2025 Special Issue April (2026) 16 - 30

FABRICATION OF GNP-PNIPAAM THERMORESPONSIVE MEMBRANE FOR TREATMENT OF OILY WASTEWATER

ELVIN KAI HONG CHUA[1], KAH CHUN HO[1,2,3,*], JIUN HOR LOW[1,2,3], YEIT HAAN TEOW[4]

[1]School of Engineering, Faculty of Innovation and Technology, Taylor's University, No. 1, Jalan Taylor's, 47500 Subang Jaya, Selangor, Malaysia.
[2]Clean Technology Impact Lab, Taylor's University, No.1, Jalan Taylor's, 47500 Subang Jaya, Selangor, Malaysia
[3]Centre for Sustainable Societies, Taylor's University, No.1, Jalan Taylor's, 47500 Subang Jaya, Selangor, Malaysia
[4]Department of Chemical and Process Engineering, Faculty of Engineering and Built Environment, Universiti Kebangsaan Malaysia, 43600 UKM Bangi, Selangor, Malaysia
*Corresponding Author: kahchun.ho@taylors.edu.my

Abstract

Kitchen wastewater containing high concentration of oil and grease leads to the clogging of sewage drains and the generation of pungent smell. Membrane stands out for the potential solution to overcome this challenge, and it can be reused by different cleaning methods. Thermo-cleaning is one of the methods can be applied to thermoresponsive membrane to overcome the major limitation in membrane technology which is membrane fouling. This study aims to explore the use of thermoresponsive membranes by adding graphene nanoplates and poly(N-isopropylacrylamide) (GNP-PNIPAAm) nanocomposite into the polyvinylidene fluoride (PVDF) membrane. Various concentration of GNP-PNIPAAm nanocomposite (0.05 wt%, 0.275 wt% and 0.50 wt%) in thermoresponsive membrane was studied. In general, the synthesized thermoresponsive membranes showed improved hydrophilicity because of the formation of hydrogen bond between the water molecules. In terms of oil rejection, thermoresponsive membrane (M3) with 0.50 wt% of GNP-PNIPAAm nanocomposite was able to maintain high oil rejection above 85% over four-cycle of filtration after thermo-cleaning. During the thermo-cleaning, M3 thermoresponsive membrane showed improved high flux recovery (85%-99%) compared to the pristine membrane (25.93%-77.78%) attributed to the membrane shrinking-swelling actuation motion during temperature-change cleaning.

Keywords: Antifouling, Flux Recovery, GNP-PNIPAAm, Oily Wastewater, Thermoresponsive membrane.

1. Introduction

Separation process by using the membrane technology is one of the most cost-effective methods for wastewater treatment. However, fouling is the main obstacle that must be solved for all the applications of membrane. For example, oil particles from the oily wastewater act as a foulant and deposit on the membrane surface [1]. The foulant reduces the permeability of water through the membrane and deteriorates the separation performance of the membrane. Various mitigation strategies such optimization of operating condition and membrane modification have been explored by the researchers. Among these strategies, modification of membrane to produce thermoresponsive membrane was suggested to overcome fouling issue [2].

Poly(N-isopropylacrylamide) (PNIPAAm) is an excellent thermoresponsive polymer which demonstrates a reversible phase transition across the polymer's lower critical solution temperature (LCST), 34 ºC [3]. When the temperature was below LCST, PNIPAAm is soluble in water and hydrated (hydrophilic) attributed to the formation of hydrogen bond between the water molecules and the amide side chains.

When the temperature was above LCST, PNIPAAm becomes insoluble in water and dehydrated (hydrophobic) owing to the disruption of the hydrogen bond with the structured water around isopropyl groups [4]. This temperature-induced phase transition of PNIPAAm repels the deposited foulant on the membrane surface when the temperature of water is adjusted below and above LCST of PNIPAAm. Hence, the efficiency of membrane filtration is enhanced as the foulant can be removed from the membrane surface easily by thermo-cleaning.

It is known the thermoresponsiveness of the PNIPAAm is dependent on the transfer of heat energy from the surrounding. Hence, nanomaterial was typically incorporated with PNIPAAm to enhance the heat transfer in the nanocomposite [5]. The enhancement of thermal conductivity in thermoresponsive polymer could lower the temperature response rate and expand the application of thermoresponsive membrane.

Recently, graphene nanoplate (GNP) attracted the attention of the researcher due to its thermal stability, mechanical strength and hydrophobic nature. GNP is also an excellent heat conductor due to its high intrinsic thermal conductivity (up to 5000 $W/m^{-1}k^{-1}$) [6]. GNP created efficient heat transfer pathways when added to nanocomposites by forming a thermally conductive networks within the material [7]. Recently, Tang et al. [8] prepared aerogel adsorbent by introducing exfoliated montmorillonite, Ti_3C_2-MXene and PNIPAAm into the carboxylated cellulose nanofibers.

The addition of Ti_3C_2 substantially improved the thermal conductivity (106 $mW/m^{-1}k^{-1}$) and temperature responsiveness of aerogel. This allows fast oil–water separation and desorption regeneration for quick response in oil cleaning. Therefore, introducing GNP-PNIPAAm nanocomposite to the fabrication of thermoresponsive membrane provides insights to fully identify their potentials and benefit in the membrane technology.

However, the specific pairing of PNIPAAm and GNP has not yet been reported. The integration of GNP-PNIPAAm could enhance the synergistic relationship by leveraging the thermoresponsive properties of PNIPAAm and the thermal

conductivity of the GNP. Hence, the objective of this research is to explore the effect of GNP-PNIPAAm nanocomposite to the performance of thermoresponsive membrane such as permeability, oil rejection and antifouling.

Various concentrations of GNP-PNIPAAm nanocomposite were studied and kitchen oil emulsion was used as model foulant in oily wastewater. Membrane thermo-cleaning was conducted for three cycles across the LCST of thermoresponsive polymer to evaluate the stability of membrane for oily wastewater treatment.

2. Materials and Methods

2.1. Materials

GNPs with thickness of 2-10 nm were supplied by ACS Material LLC, USA. 4 M nitric acid (HNO_3) from Chemiz, Malaysia and 30% hydrogen peroxide (H_2O_2) from Systerm, Malaysia were used to oxidize GNP. 99.8% ethanol absolute from BDH UK 99% 3-methacryloxypropyl trimethoxysilane (MPS) by Macklin, China, acetic acid, and acetone were used for silanization. 98% N-isopropyl acrylamide (NIPAAm) and N,N′-Methylenebis(acrylamide) (MBA) supplied by Macklin, China while 99% dimethylacetamide (DMAc) from Merck, Germany, and potassium persulfate (KPS) from Sigma-Alrich, Germany were used for radical polymerization. Polyvinylidene fluoride (PVDF) T-1 from Shanghai Ofluorine Co., China was used for membrane synthesis. SAJI palm cooking oil supplied by Delima Oil Products Sdn. Bhd. Malaysia and sodium dodecylbenzenesulfonate (SDBS) supplied by Sigma, Germany were used to prepare kitchen oil emulsion.

2.2. Synthesis of GNP-PNIPAAm nanocomposite

2.2.1. Preparation of oxidized GNP (GNP-OX)

0.5 g of GNP was added to 175 mL of HNO_3 (3M) solutions and stirred at 60 °C and 250 rpm for 15 minutes [9]. This mixture was sonicated at frequency of 80 kHz for 30 minutes using ultrasonicator (P120H, Elmasonic, Germany) to homogenize GNP in HNO_3 solution. The mixture was then rinsed with the distilled water and underwent centrifugal washing. The obtained GNP was mixed together with 175 mL of H_2O_2 (30%) solution and previous steps were repeated. Oxidized GNP (GNP-OX) was dried using freeze dryer (ScanVac Coolsafe Touch 110-4, Labogene, Denmark) at -100 °C for 1 day.

2.2.2. Preparation of GNP-MPS

400 mL of deionized (DI) water and ethanol mixture was prepared at 20:80% v/v. The pH of the mixture was adjusted to a range of 3.5 to 4.5 using acetic acid for silanization of GNP-OX [10]. 2 g of MPS was added into the mixture and stirred for 20 minutes under ambient temperature. Then, 0.5 g of GNP-OX was added into this mixture and sonicated at frequency of 80 kHz using the ultrasonicator (P120H, Elmasonic, Germany) for 1 hour. GNP-MPS mixture was then stirred at 60 °C and 250 rpm for 4 hours. Acetone and distilled water were used to rinse the mixture for three times. Finally, GNP-MPS was dried using freeze dryer (ScanVac Coolsafe Touch 110-4, Labogene, Denmark) at -100 °C for 1 day.

2.2.3. Preparation of GNP-PNIPAAm nanocomposite

To synthesize the thermoresponsive GNP-PNIPAAm nanocomposite, 0.5 g of GNP-MPS, 2.5 g of NIPAAm and 0.15 g of MBA were added into a 300 mL DI water and DMAc mixture at ratio of 50:50% v/v [11]. Afterwards, the mixture was sonicated at frequency of 80 kHz using the ultrasonicator (P120H, Elmasonic, Germany) for 30 minutes. After that, the mixture was mixed at 70ºC under nitrogen atmosphere for 24 hours. 0.1 g of KPS was added into the mixture as polymerization initiator. Radical polymerization was conducted at 70 ºC with vigorous stirring for another 24 hours. Successively, the resulted mixture was washed with DI water for at least three times. Dried GNP-PNIPAAm nanocomposite was obtained using freeze dryer (ScanVac Coolsafe Touch 110-4, Labogene, Denmark) at –100 °C for 1 day.

2.3. Synthesis of GNP-PNIPAAm thermoresponsive membrane

Various concentrations of GNP-PNIPAAm nanocomposite were dispersed into DMAc as shown in Table 1 (with respect to PVDF weight). The GNP-PNIPAAm nanocomposite was dispersed at frequency of 80 kHz for 30 minutes using ultrasonicator (P120H, Elmasonic, Germany). Then, PVDF was added into the dispersion and stirred at 60 ºC and 500 rpm for 4 hours. After that, the mixture was stirred again at 40 ºC and 500 rpm for another 4 hours to ensure the PVDF fully dissolved in the mixture [12].

The membrane polymer solution was casted evenly as thin film onto a flat non-woven polyester membrane support (CU414 Opti, Neenah US) which was secured to a glass plate. The membrane thickness was controlled at 200 μm using an adjustable film applicator. The glass plate with membrane polymer film was submerged in 5 L distilled water bath for one day to complete the phase inversion. Finally, the synthesized thermoresponsive membranes were removed from the water bath and stored in distilled water at 4 °C.

Table 1. Composition of GNP-PNIPAAm nanocomposite in thermoresponsive membrane.

Membrane	PVDF (wt%)	DMAc (wt%)	GNP-PNIPAAm nanocomposite (wt%)
M0	18	82	0.000
M1	18	82	0.050
M2	18	82	0.275
M3	18	82	0.500

2.4. Nanocomposite and membrane characterization

2.4.1. FTIR for Nanocomposite

The chemical bonding of GNP and GNP-PNIPAAm nanocomposite was recorded by the attenuated total reflectance (ATR)-Fourier transform infrared (ATR-FTIR) spectra on the Spectrum 65 FTIR spectrometer, PerkinElmer, USA. A small amount of nanocomposite sample was placed on the scanning area. A metal tip was pressed against the crystal to fix the sample. The spectra were scanned from 400 cm^{-1} to 4000 cm^{-1} at 4 cm^{-1} scan resolution and 16-scan accumulation [13].

2.4.2. Membrane porosity and pore size

The porosity of the membrane was calculated using gravimetric method while the pore size of the membrane was calculated by Guerout-Elford-Ferry equation [14]. The fabricated membrane was soaked in the distilled water to ensure the pores were filled with water. After that, the membrane was cut into small piece of 1 cm × 1 cm and weighed. The wet membrane was dried at 50 °C for one day to eliminate the water molecule. The dried membrane was then weighed again afterwards. Membrane pore radius and porosity were determined using Eqs. (1) and (2) [15].

$$\varepsilon = \frac{\frac{\omega_1-\omega_2}{\rho_\omega}}{\frac{\omega_1-\omega_2}{\rho_\omega}+\frac{\omega_2}{\rho_\rho}} \times 100\% \quad (1)$$

where ε is the porosity of membrane (%), ω_1 and ω_2 is the weight of membrane before and after drying process (g), ρ_w is the density of water at 25 °C (0.998 g/mL) while ρ_ρ is the density of PVDF at 25 °C (1.765 g/mL).

$$r_m = \sqrt{\frac{(2.9-1.75\varepsilon)*8V\mu\delta}{\varepsilon PA}} \quad (2)$$

where r_m is the mean pore radius of the membrane, V refers to the volumetric flow rate of water (m^3/s), μ represents the dynamic viscosity of water at 25 °C (0.891 mPa.s), δ is the thickness of the membrane (m), A is the area of membrane (m^2), P is the operating pressure of the system (Pa) and ε is the thickness of the membrane (m).

2.4.3. Membrane hydrophilicity

A contact angle goniometer (OCA 15EC, DataPhysics Instruments, Germany) was utilized to perform the water contact measurement via sessile drop method [16]. This is to assess the hydrophilicity of the membrane surface. Around 1 µL of water droplet was gently dispensed on the membrane surface and three measurements were conducted to obtain an average value.

2.4.4. Membrane morphology study

Scanning Electron Microscope (Hitachi TM3000, Tokyo, Japan) was used to examine the top surface and cross-sectional morphologies of the membranes [17]. To examine the top surface morphology, the membranes were cut and observed in area of 0.5 cm × 0.5 cm with 15.0 kV. For cross-sectional view, the membrane samples were cryo-fractured using liquid nitrogen. Magnification of 8 k× and 10 k× were used for imaging.

2.5. Membrane performance

A dead-end membrane filtration cell (16249, Sartorius Stedim Biotech, Germany) was used to examine the performance of membrane in the treatment of kitchen oil emulsion. The membrane with effective area of 13 cm^2 with a diameter of 47 mm was prepared [18].

2.5.1. Permeability of pure water

In order to lower down the impact of compaction, the fabricated membrane was pre-pressurized under a fixed pressure of 3 bar for 30 minutes to obtain a constant

flux [19]. Distilled water was used to filter the membrane to obtain the permeate flux. At the same time, transmembrane pressure (TMP) was adjusted at 1.0, 1.5 and 2.0. The permeate flux of membrane was calculated by Eq. (3); the permeability of the membrane was determined by the gradient of permeate flux against TMP.

$$J = \frac{\Delta V}{A \Delta t} \quad (3)$$

where ΔV is the volume of permeate (L) while J represented the permeate flux ($Lm^{-2}h^{-1}$). Δt represented membrane permeation period (h) while A is the effective surface area of the membrane (m^2).

2.5.2. Oil rejection

50 mg of SDBS was added to the 50 mL kitchen oil-water mixture with kitchen oil concentration of 1 wt% [20]. The kitchen oil-water mixture was then dispersed using processors ultrasonic (CP/OO/O/P-04711-45, Cole Parmer, USA) at 750 W and 20 kHz for 2 min to prepare kitchen oil emulsion [20]. Oil rejection of the fabricated membrane was investigated by using kitchen oil emulsion as the feed solution to the membrane. The concentration of kitchen oil emulsion was determined by using UV/VIS spectrophotometer (Spectroquant® Prove 300, Merck, Germany) at wavelength of 261 nm. Rejection of oil was measured by Eq. (4) [21].

$$R = \left(1 - \frac{C_p}{C_f}\right) \times 100\% \quad (4)$$

where R is the rejection factor (%), C_P is the concentration of kitchen oil emulsion after filtration, C_f is the concentration of kitchen oil emulsion before filtration.

2.5.3. Fouling study and thermo-cleaning study

After 15 minutes of kitchen oil emulsion filtration, membrane was removed from the membrane filtration cell and underwent thermo-cleaning. The membranes were immersed in distilled water at 40 °C and 25 °C for 10 minutes each [4]. Then, the kitchen oil emulsion filtration was repeated. A total of three cycles of membrane thermo-cleaning was conducted. Fouling behaviour of each fabricated membrane was investigated by Eq. (5) with normalized flux over filtration period.

$$\text{Normalized Flux} = \frac{J_1}{J} \quad (5)$$

where J is the flux of distilled water while the J_1 is the flux of kitchen oil emulsion.

3. Results and Discussion

3.1. Presence of functional group on nanocomposite

Figure 1 shows the infrared spectra of GNP and GNP-PNIPAAm nanocomposite. GNP has no noticeable peak which is consistent with other study [22]. Whereas for GNP-PNIPAAm nanocomposite, two broad absorption peaks at 3417 cm^{-1} and 1049 cm^{-1} assigned to the hydroxyl (O−H) and C−O stretching vibration were observed. This is due to the oxidation of GNP during the synthesis of GNP-PNIPAAm. Besides, the peak at 1651 cm^{-1} given to the stretching vibration of amide (−NH) I resulted from PNIPAAm [23]. The small peak with value of 2971

cm^{-1} contributed by methylene group which can be found in PNIPAAm [10]. All these functional groups confirmed the successful bonding of PNIPAAm to the GNP.

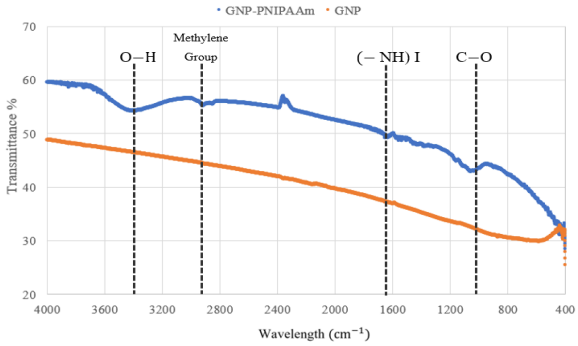

Fig. 1. FTIR results of GNP and GNP-PNIPAAm nanocomposite.

3.2. Characterization of membrane

3.3.1. Membrane porosity and pore size

The porosity and pore radius of the fabricated membrane are summarized in Table 2. The porosity of these membranes has a range from 75.47% to 89.26% while the pore size of the membranes is ranged from 10.26 nm to 19.13 nm. As shown, the mean porosity of the thermoresponsive membrane started to decrease from 89.26 % to 75.47 % for the membrane (M0 to M3) with increasing concentration of GNP-PNIPAAm nanocomposite from 0 wt% to 0.50 wt%. The presence of GNP leads to the reduced porosity in thermoresponsive membrane as GNP tend to self-align their basal planes during the membrane phase inversion, thus creating a compact packing membrane structure [24]. Additionally, the tendency of the GNP to interfere and agglomerate is clearly proportional to the concentration of the GNP inside the thermoresponsive membrane, and this led to a lower porosity.

Table 2. Porosity and mean pore radius of membrane.

Membrane	Porosity, ε (%)	Mean pore radius, r_m (nm)
M0	89.26 ± 6.17	19.13 ± 1.41
M1	88.88 ± 2.42	17.84 ± 0.52
M2	79.10 ± 6.11	14.82 ± 1.13
M3	75.47 ± 5.24	10.26 ± 0.65

Regarding to the pore size, the addition of the GNP-PNIPAAm nanocomposite decreases the pore radius as shown in Table 2. Pristine M0 membrane has shown the highest value of the pore radius as it only consists of PVDF polymer without any addition of the nanocomposite. The decreasing of the pore size can be explained as the nanocomposite tend to pack more tightly together in a higher concentration within membrane matrix. This dense stacking resulted less space between the layers and formation of smaller pores within the thermoresponsive membrane. Thus, permeability of the water was lower due to the pathways for water molecules to pass through becoming more constricted which will be further explained in Section 3.3.1.

3.3.2. Water contact angle

As shown, the M0 membrane has a contact angle of 69.01±7.22º and slightly hydrophilic (<90º). A decreasing trend of the contact angle (57.17±8.15º - 69.24±6.46º) can be observed after adding the GNP-PNIPAAm nanocomposite. In comparison to the pristine PVDF membrane (M0), presence of the GNP-PNIPAAm nanocomposite increases hydrophilicity of the thermoresponsive membrane. This is because of the presence of oxygen functional groups and allows the membranes to form hydrogen bonds with water molecules as shown in FTIR spectra (Fig. 2).

Besides, the water contact angle measurement was carried out at room temperature which is below LCST of PNIPAAm. Hence, higher concentration of GNP-PNIPAAm nanocomposite in the membrane increases the high surface free energy of the thermoresponsive membranes. This high surface free energy increased surface hydrophilicity and overall moisture absorption ability of the membrane. Xiong and Ulbricht [25] reported that the surface free energy for PVDF membrane increased from 64.6 mN/m to 73.7 mN/m when the PNIPAAm grafting yield increased from 11.2% to 35.3% at 25°C.

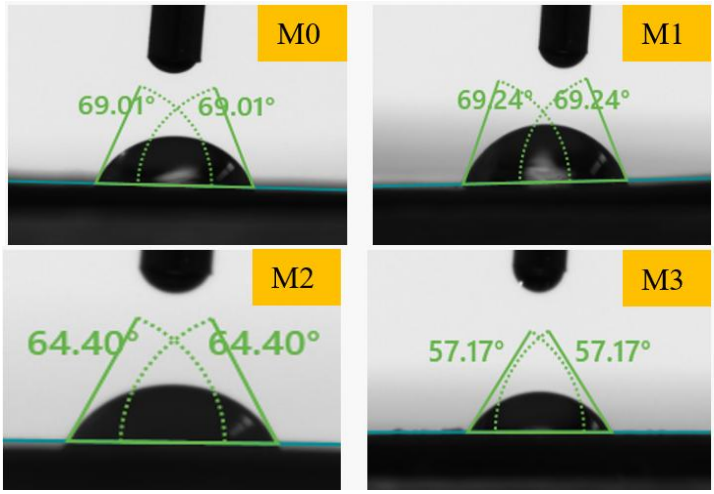

Fig. 2. Water contact angle for membrane.

3.3. Membrane performance

3.3.1. Permeability

The water permeability of membrane was illustrated in Fig. 3. As shown, M0 membrane has the highest water permeability (65.93 $Lm^{-2}h^{-1}bar^{-1}$) while M3 thermoresponsive membrane had the lowest water permeability (9.45 $Lm^{-2}h^{-1}bar^{-1}$). This trend aligns with the results of the porosity/pore size where M0 membrane has the highest porosity/pore size while M3 thermoresponsive membrane has the lowest porosity/pore size as presented in Table 2. Permeability defines the ease of a fluid to move through a medium which is strongly affected by the porosity/pore size of the medium. Larger porosity/pore size typically enable more fluid to pass through due to its properties of higher porosity/pore size with lower flow resistance and end up with higher permeability.

However, the water permeability result was contradicting with the water contact angle reported in Fig. 2. It was expected that the M3 thermoresponsive membrane with the highest surface hydrophilicity foster a stronger interaction with the water molecules resulted greater water flux through the membrane. Nevertheless, it was not observed in this work as the great reduction in membrane porosity/pore size has more dominant impact on water permeability than the surface hydrophilicity. This is consistent with mathematical modelling by Rabiei and Paterson [26], membrane with larger pore sizes result in lower liquid entry pressure and causing membranes more readily to pore wetting thereby enhancing membrane permeability.

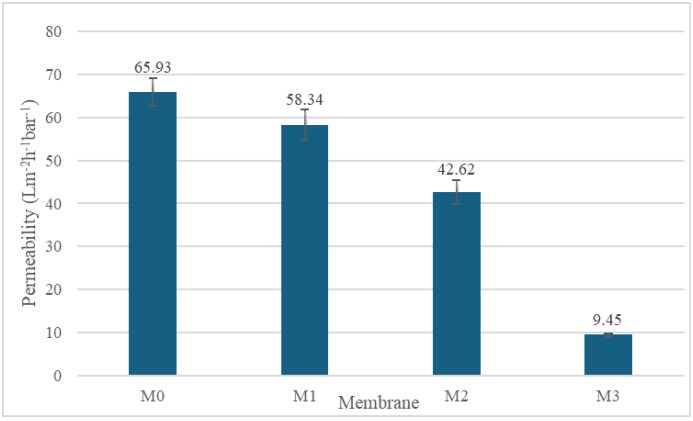

Fig. 3. Permeability of membrane.

This was also witnessed by the top surface and cross-sectional images of pristine M0 membrane and thermoresponsive nanocomposite membrane (M1 and M3). For the top surface images, pristine M0 membrane showed more porous surface (represented by the dark spots) (Fig. 4(a)) compared to the M1 and M3 thermoresponsive membrane (Figs. 4(b) and (c)). This observation also supports the decreased membrane porosity by thermoresponsive membrane reported in Table 2. In terms of the cross-sectional images, pristine M0 membrane showed a thinner skin layer (Fig. 4(d)) compared to M1 and M3 thermoresponsive membrane (Figs. 4(e) and (f)).

Besides, the addition of low concentration of GNP-PNIPAAm nanocomposite (0.05 wt%) increases the sizes of macro voids due to the hydrophilicity of the casting solution. However, further increase of the concentration of GNP-PNIPAAm nanocomposite (0.50 wt%) prevented the formation of large macro voids. This could be due to the agglomeration of GNP-PNIPAAm nanocomposite thus delayed on phase inversion process [10].

3.3.2. Fouling study

Figure 5 shows the normalized flux of the membranes over the four-cycle of kitchen oil emulsion filtration at 3 bars. At the end of first filtration cycle, the M3 thermoresponsive membrane achieved the highest normalized flux (0.6000) while the lowest normalized flux (0.1944) was attained by M1 thermoresponsive membrane. This can be explained by the water contact angle or surface hydrophilicity of the thermoresponsive membranes presented in Fig. 2.

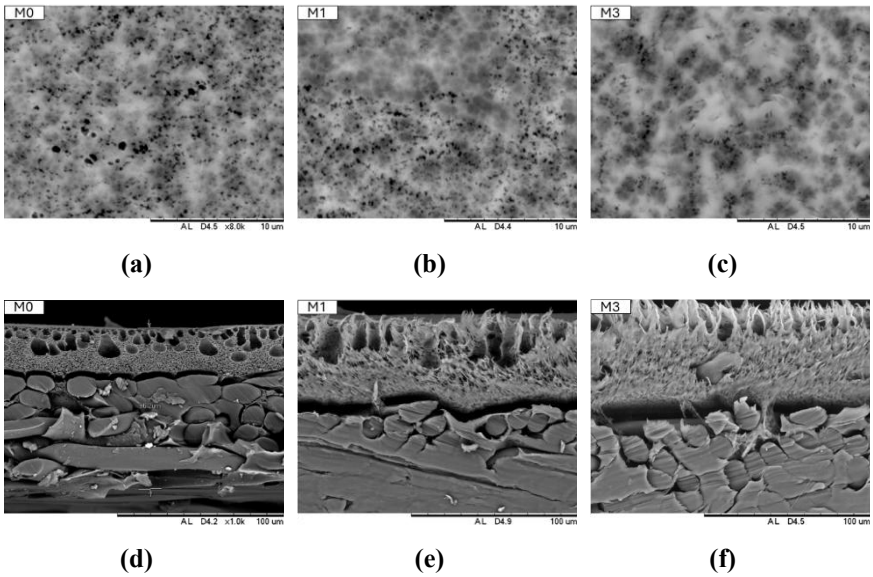

Fig. 4. Membrane top surface (a, b, c) (8 k×) and cross-sectional images (d, e, f) (1 k×) morphology.

M3 thermoresponsive membrane has the lowest mean water contact angle (57º) among all the membranes indicated high surface hydrophilicity. As the membrane fouling mainly is owing to the hydrophobic interactions between oil and hydrophobic surface of the membrane, the thermoresponsive membrane with presence of hydrophilic functional groups exhibited antifouling properties when the membrane is exposed to the oil solution.

The hydrophilic membrane surface reduces oil attachment and therefore effectively alleviates permeation flux decline. For instance, Xie et al. [27]. reported the blending of sulfonated polysulfone into polyvinyl chloride matrix substantially improved membrane hydrophilicity which resulted in the enhancement of antifouling property against bovine serum albumin with high flux recovery ratio (96%). This is owing to the formation of hydration layer by hydrophilic segments segregate on the membrane surface thus avoiding the adsorption of the foulant.

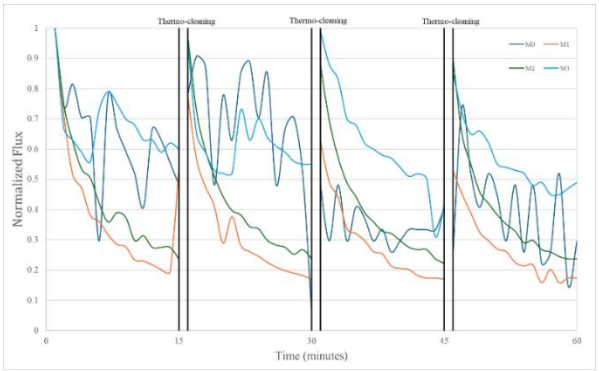

Fig. 5. Recovery of flux for membrane.

After membrane thermo-cleaning with water at 40 °C and 25 °C for 10 minutes, all membrane flux recovered in the range of 77.78 % to 97.71 % in the second filtration cycle. Simple water cleaning removed the oil accumulated on the membrane surface hence the membrane flux could be recovered. Both pristine M0 membrane and M1 thermoresponsive membrane exhibited lower flux recovery of 77.78% mainly due to absence or minimal amount of GNP-PNIPAAm nanocomposite for effective thermo-cleaning. Hence, the oil is challenging to be washed away by distilled water, and the membrane flux recovery is limited.

On the other hand, M2 and M3 thermoresponsive membrane showed excellent efficiency of cleaning with almost complete flux recovery (97.71 % and 96.00%) in the second cycle. This could be due to the membrane shrinking-swelling actuation motion during thermo-cleaning at 40 °C/25 °C. This thermo-cleaning mechanism created actuation force and loosened the fouling layer on membrane surface effectively. At 40 °C, the chains of GNP-PNIPAAm nanocomposite were shrunken causing the release of water molecules which reducing the adsorption of oil.

Whereas, at 25 °C, the chains of GNP-PNIPAAm nanocomposite were restored to swollen state resulting in adsorption of water molecules forming hydration layer. Comparable result was obtained by Mao et al. [28] using thermoresponsive membrane synthesized by blending grafted PNIPAAm-attapulgite with PVDF polymer. It was reported 89% of biofouling on thermoresponsive membrane surface was achieved by a temperature-change coupling ultrasonic cleaning process. This is attributed to switching of polymer chains between contraction and hydrophobic state to stretching and hydrophilic state during temperature-change cleaning.

In the third and fourth filtration cycle, both pristine M0 membrane and M1 thermoresponsive membrane further experienced deterioration in membrane flux with flux recovery ranged from 25.93-48.15% and 52.78-62.70%, respectively. This is because of the development of thicker cake layer on the membrane surface and caused more oil blockage inside the membrane pores due to the ineffective membrane cleaning [29].

On the contrary, the performance of M2 and M3 thermoresponsive membrane remained high as 87.79-89.31% and 85-99%, respectively. Particularly, M3 thermoresponsive membrane maintained high flux recovery and stable operation throughout the four-filtration cycles. This also confirms that the thermal phase transition of the thermoresponsive polymer chains was reversible across the phase transition temperature.

3.3.3. Oil rejection

Figure 6 depicts the oil rejection of the membrane over four-cycles of the kitchen oil emulsion filtration. In general, the membrane rejection is high in the first cycle ranging from 89.60 % to 93.02 %. The high oil rejection in the first cycle is primarily due to the pore radius of the membrane as shown in Table 2. It was reported that average droplet emulsion droplet size ranges from 33 to 142 nm depending on nature and concentration of surfactant, the characteristics of both the dispersed and the continuous phase, and the preparation method [30]. Based on the sieving principle of pore size, the membranes with small pore radius (10.26-19.13 nm) can effectively separate the emulsion (Table 2).

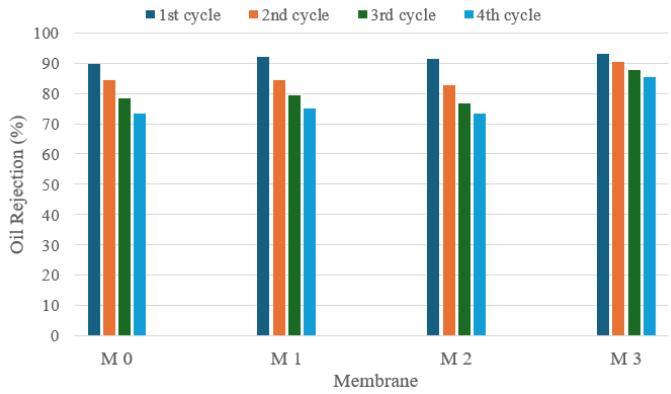

Fig. 6. Oil rejection of membrane.

After membrane cleaning with distilled water at 40 ºC and 25 ºC, the membrane oil rejection decreased to 84.46-90.46%, 76.80-87.89%, and 73.38-85.34% in the subsequent filtration cycle. This could be caused by the adhesion of the oil residues on the membrane surface or membrane pore after cleaning with different water temperature. This is better known as irreversible fouling and the oil residues are trapped inside the pores of membrane overtime.

It is observed that membranes with bigger pore sizes (M0, M1, M2) suffered severe drop in oil rejection (16.22-17.94%) while membrane with smaller pore size (M3) experienced moderate drop in oil rejection (7.68%). This could be due to the tendency of oil to be trapped inside the bigger membrane pores affecting the cleaning efficiency and the oil could pass through the membrane. In short, M3 thermoresponsive membrane has a more stable performance compared to other membranes in filtration cycle with minimum loss.

4. Conclusion

In summary, this research investigated the effect of GNP-PNIPAAm nanocomposite concentration on the structural and functional properties of thermoresponsive membranes. Kitchen oil emulsion was used as model foulant for oily wastewater treatment. As reported, the increased GNP-PNIPAAm nanocomposite concentration (0.05 wt%-0.50 wt%) had reduced the membrane porosity and pore size while enhanced membrane hydrophilicity because of the oxygen functional groups on GNP-PNIPAAm.

The top surface and cross-sectional images of membranes further supported the reduced surface porosity and thicker skin layer in the thermoresponsive membrane. As a result, the thermoresponsive membranes showed reduction in water permeability (9.45-58.34 $Lm^{-2}h^{-1}bar^{-1}$) compared to the pristine membrane (65.39 $Lm^{-2}h^{-1}bar^{-1}$). Nevertheless, all thermoresponsive membranes demonstrated excellent performance in terms of oil rejection and flux recovery during kitchen oil emulsion filtration. Particularly, M3 thermoresponsive membrane with 0.50 wt% of GNP-PNIPAAm nanocomposite showed high oil rejection (85.34%-93.02%) and flux recovery (85%-99%) during the four-filtration cycle.

This stable membrane performance mainly attributed to the effective membrane thermo-cleaning by membrane shrinking-swelling actuation motion which loosened the fouling layer on membrane surface. The research provides insights into the effect of GNP-PNIPAAm nanocomposite concentration on the performance of thermoresponsive membrane for potential oily wastewater treatment. By leveraging on the thermoresponsive properties of PNIPAAm and the thermal conductivity of the GNP, the thermoresponsive membrane, further research could be conducted to examine the membrane thermoresponsiveness by manipulating cleaning period and temperature.

Acknowledgements

The authors wish to gratefully acknowledge the financial support by Taylor's University through Taylor's Internal Research Grant Scheme - Impact Lab Grant (TIRGS-ILG) (Project Code: TIRGS-ILG/2/2024/SOE/001).

References

1. Gupta, U.; Urmaliya, D.N.; Madhav, S.; and Jindal, T. (2025). Remediation of oil contamination from sewage treatment plant membranes using advanced technologies in the current scenario. *Sustainable Chemistry for Climate Action*, 6, 100080.
2. Ho, K.C.; and Low, J.H. (2025). Recent advances in thermoresponsive materials for water and wastewater treatment. *Journal of Environmental Chemical Engineering*, 13(6), 120053.
3. Lam, A.X.; Teow, Y.H.; and Ho, K.C. (2021). Effect of monomers for the synthesis of chitosan-based hydrogel. *International Journal of Nanoelectronics and Materials*, 14(2), 113-126.
4. Ngang, H.P.; Ahmad, A.L.; Low, S.C.; and Ooi, B.S. (2017). Preparation of thermoresponsive PVDF/SiO_2-PNIPAM mixed matrix membrane for saline oil emulsion separation and its cleaning efficiency. *Desalination*, 408, 1-12.
5. Zhao, J.; Xue, Y.; Wu, Y.; Hao, X.; Sun, S.; and Zhang, H. (2025). Core-shell BN@PDA-Ag embedded PVDF-PNIPAAm/CS@CNT dual-layer membrane by electrospun with photothermal-triggered self-cleaning and adaptive filtration for high-flux water treatment. *Chemical Engineering Journal*, 515, 163586.
6. Zhang, C. et al. (2025). Preparation of graphene nanoplatelets reinforced aluminum matrix composites by friction stir processing and study of thermal conductivity and toughness properties. *Materials Today Communications*, 48, 113606.
7. Chen, Q. et al. (2026). Low-cost, scalable, thermally conductive polymer nanocomposite films for dual-mode battery thermal management. *Journal of Materials Science & Technology*, 254, 145-155.
8. Tang, R. et al. (2024). Fast-thermoresponsive carboxylated cellulose nanofibers/Ti_3C_2/exfoliated montmorillonite-poly(N-isopropylacrylamide) with switchable wettability for oil-water separation. *Separation and Purification Technology*, 339, 126580.
9. Ho, K.C.; Chan, M.K.; Chen, Y.M.; and Subhramaniyun, P. (2023). Treatment of rubber industry wastewater review: Recent advances and future prospects. *Journal of Water Process Engineering*, 52, 103559.

10. Yaghoubi, Z.; and Parsa, J.B. (2019). Preparation of thermo-responsive PNIPAAm-MWCNT membranes and evaluation of its antifouling properties in dairy wastewater. *Materials Science and Engineering*: *C*, 103, 109779.
11. Yaghoubi, Z.; and Basiri-Parsa, J. (2020). Modification of ultrafiltration membrane by thermo-responsive Bentonite-poly(N-isopropylacrylamide) nanocomposite to improve its antifouling properties. *Journal of Water Process Engineering*, 34, 101067.
12. Goh, T.W.; Ho, K.C.; Teow, Y.H.; and McGarry, K. (2023). Influence of rGO/MWCNTs on antifouling properties of nanocomposite membrane: Statistical analysis. *IP Conference Proceedings*, 2847(1), 020014.
13. Vásquez, L.; Campagnolo, L.; Athanassiou, A.; and Fragouli, D. (2019). Expanded graphite-polyurethane foams for water-oil filtration. *ACS Applied Materials & Interfaces*, 11(33), 30207-30217.
14. Chan, M.K.; Ong, C.S.; and Kumaran, P. (2018). Development and characterization of glycerol coating on the PAN/PVDF composite membranes. *IOP Conference Series*: *Materials Science and Engineering*, 458, 012006.
15. Nik Abdul Ghani, N.R.; Jami, M.S.; Engliman, N.S.; Amosa, M.K.; and Isa, M.H. , M.H. (2021). Study of graphene oxide-polymer nanocomposite (GPN) adsorptive membrane for lead removal from wastewater. *Journal of Engineering Science and Technology*, 16(5), 3620-3636.
16. Patil, D.; Muthaiah, V.M.S.; Chandru, M.; Stoller, M.; and Chatterjee, K. (2026). Electrochemical dealloying of a titanium alloy yields hierarchical surface topography with mechanobactericidal activity. *Next Materials*, 10, 101456.
17. Mohamed Noor, S.H.; Othman, M.H.D.; Khongnakorn, W.; Sinsamphanh, O.; Abdullah, H.; Puteh, M.H.; Kurniawan, T.A.; Zakria, H.S.; El-Badawy, T.; Ismail, A.F.; Rahman, M.A.; and Jaafar, J. (2022). Bisphenol a removal using visible light driven Cu_2O/PVDF photocatalytic dual layer hollow fiber membrane. *Membranes*, 12(2), 208.
18. Teow, Y.H.; Ho, K.C.; Wickramasinghe, S.R.; Jebur, M.G.; and Chang, Z.H. (2022). *Integrated process technology for recycling and re-use of industrial and municipal wastewater*: *A review*. In Kumar, V.; and Kumar, M. (Eds.), *Integrated environmental technologies for wastewater treatment and sustainable development*. Elsevier, 49-80.
19. Nik Abdul Ghani, N.-R.; Jami, M.S.; Alam, M.Z.; and Engliman, N.-S. (2023). Investigation of fouling mechanism on graphene oxide polyethersufone nanocomposite adsorptive membrane. *Journal of Engineering Science and Technology*, 18(5), 2672-2687.
20. Chen, J.; Sun, M.; Ni, Y.; Zhu, T.; Huang, J.; Li, X.; and Lai, Y. (2023). Superhydrophobic polyurethane sponge for efficient water-oil emulsion separation and rapid solar-assisted highly viscous crude oil adsorption and recovery. *Journal of Hazardous Materials*, 445, 130541.
21. Ho, K.C.; Teow, Y.H.; Ang, W.L.; and Mohammad, A.W. (2017). Novel GO/OMWCNTs mixed-matrix membrane with enhanced antifouling property for palm oil mill effluent treatment. *Separation and Purification Technology*, 177, 337-349.
22. Banou, M.; Niu, Y.; Ammari, F.; Dunlop, T.; Palmer, R.E.; and Tizaoui, C. (2023). Fabrication of graphene nanoplatelets/MgAl-layered double hydroxide

nanocomposites as efficient support for gold nanoparticles and their catalytic performance in 4-nitrophenol reduction. *Process Safety and Environmental Protection*, 174, 891-900.

23. Tan, J.; Yang, Q.; Hu, G.; Zhang, H.; Pei, L.; and Wang, J. (2022). Experimental study on the temperature-sensitive behavior of poly-n-isopropylacrylamide/graphene oxide composites and the flexible conductive cotton fabrics. *Polymer Testing*, 110, 107563.
24. Kumarao, P.; Ho, K.C.; Low, J.H.; Teh, J.L.; and Teow, Y.H. (2026). Study of antifouling properties of MWCNTs/GNPs nanocomposite membrane against BSA protein. *Journal of Engineering Science and Technology*, Special Issue (23rd EURECA 2025), 95-109.
25. Xiong, C.; and Ulbricht, M. (2024). Thermally responsive porous membranes with both switching wettability and permeability prepared via grafting-to and grafting-from methods. *Chemical Engineering Research and Design*, 209, 2-11.
26. Rabiei, S.; and Paterson, A.H.J. (2025). The effect of membrane surface hydrophobicity on the performance and water production cost of a desalination unit. *Membranes*, 15(2), 63.
27. Xie, Y.-X.; Wang, K.-K.; Yu, W.-H.; Cui, M.B.; Shen, Y.-J.; Wang, X.-Y.; Fang, L.F.; and Zhu, B.-K. (2020). Improved permeability and antifouling properties of polyvinyl chloride ultrafiltration membrane via blending sulfonated polysulfone. *Journal of Colloid and Interface Science*, 579, 562-572.
28. Mao, H.; Zhou, S.; Shi, S.; Xue, A.; Li, M.; Cai, J.; Zhao, Y.; and Xing, W. (2022). Anti-fouling and easy-cleaning PVDF membranes blended with hydrophilic thermo-responsive nanofibers for efficient biological wastewater treatment. *Separation and Purification Technology*, 281, 119881.
29. Qin, H.-J.; Zhu, M.; Ji, S.; Wu, R.; Yamamoto, Y.; Qin, Y.; and Li, Y.-Y. (2025). Fouling dynamics varied by filtration cycles in high-solid anaerobic membrane bioreactors for sewage sludge treatment. *Journal of Environmental Management*, 392, 126659.
30. Onaizi, S.A. (2022). Characteristics and pH-responsiveness of SDBS-stabilized crude oil/water nanoemulsions. *Nanomaterials*, 12(10), 1673.